AGU PUBLICATIONS

JGR

Journal of Geophysical Research: Earth Surface

RESEARCH ARTICLE
10.1002/2015JF003698

Key Points:
- Traveling sticky patches produce overturning vortices in the lower part of the ice column
- The dimensions of the vortices are determined by regional slip rate and patch propagation velocity
- Observations of englacial stratigraphy can be used to constrain the history of basal slip

Correspondence to:
M. J. Wolovick,
wolovick@princeton.edu

Citation:
Wolovick, M. J., and T. T. Creyts (2016), Overturned folds in ice sheets: Insights from a kinematic model of traveling sticky patches and comparisons with observations, *J. Geophys. Res. Earth Surf.*, *121*, doi:10.1002/2015JF003698.

Received 17 AUG 2015
Accepted 13 APR 2016
Accepted article online 2 MAY 2016

Overturned folds in ice sheets: Insights from a kinematic model of traveling sticky patches and comparisons with observations

Michael J. Wolovick[1,2] and Timothy T. Creyts[1]

[1]Lamont-Doherty Earth Observatory, Columbia University, Palisades, New York, USA, [2]Department of Atmospheric and Oceanic Sciences, Princeton University, Princeton, New Jersey, USA

Abstract Overturned folds are observed in regions of the Greenland ice sheet where driving stress is highly variable. Three mechanisms have been proposed to explain these folds: freezing subglacial water, traveling basal slippery patches, and englacial rheological contrasts. Here we explore how traveling basal sticky patches can produce overturned folds. Transitions from low to high stress cause a tradeoff in ice flow between basal slip and internal deformation that deflects ice stratigraphy vertically. If these transitions move, the slip-deformation tradeoff can produce large folds. Those folds record the integrated effects of time-varying basal slip. To understand how dynamic changes in basal slip influence ice sheet stratigraphy, we develop a kinematic model of ice flow in a moving reference frame that follows a single traveling sticky patch. The ice flow field forms a vortex when viewed in the moving reference frame, and this vortex traps ice above the traveling patch and produces overturned folds. Sticky patches that travel downstream faster produce larger overturned folds. We use the model as an interpretive tool to infer properties of basal slip from three example folds. Our model suggests that the sticky patches underneath these folds propagated downstream at rates between one half and the full ice velocity. The regional flow regime for the smaller two folds requires substantial internal deformation whereas the regime for the largest fold requires substantially more basal slip. The distribution and character of stratigraphic folds reflect the evolution and propagation of individual sticky patches and their effects on ice sheet flow.

1. Introduction

Large irregular stratigraphic folds in the lower part of the ice sheet have been observed in radar data from both Greenland [*Bell et al.*, 2014; *MacGregor et al.*, 2015a] and Antarctica [*Bell et al.*, 2011]. The deformation in the lower part of the ice sheet disturbs the overlying strata into anticlines, synclines, and overturned folds. The vertical amplitude of the folds ranges from the lower limit of radar detectability to over a kilometer or about half the ice thickness (Figure 1).

The overturned stratigraphic folds in Greenland occur in regions where driving stress shows a repeating rib-like structure [*Sergienko et al.*, 2014]. Results from geophysical inversions show similar patterns in basal drag. A series of ribs contains elongated patches of strong bed oriented oblique to flow within a larger weak-bedded region. Individual patches have widths of 2–6 ice thicknesses and lengths of 5–30 ice thicknesses. The exact locations and dimensions of the basal ribs are unknown because of limitations in the inversion process, but the ribbed structure of driving stress is a robust result that depends only on ice sheet geometry from standard elevation products [e.g., *Bamber et al.*, 2013; *Fretwell et al.*, 2013].

A consequence of patchy basal drag and driving stress is that the ice flow regime must trade off between internal deformation and basal slip. When basal drag is low but velocity is high, the entire ice sheet slides in plug flow over the bed. For the same velocity, high basal drag causes high shear stresses within the lower portion of the ice column, leading the ice to flow by internal deformation. Internal deformation produces a shear layer in the lower third of the ice column where velocity varies rapidly with depth, and a thick mass of ice higher in the column moving quickly downstream at a nearly uniform rate [*Dansgaard and Johnson*, 1969]. Here we show how the tradeoff between basal slip and internal deformation associated with a sticky patch can produce overturned stratigraphic folds if the sticky patch moves downstream over time.

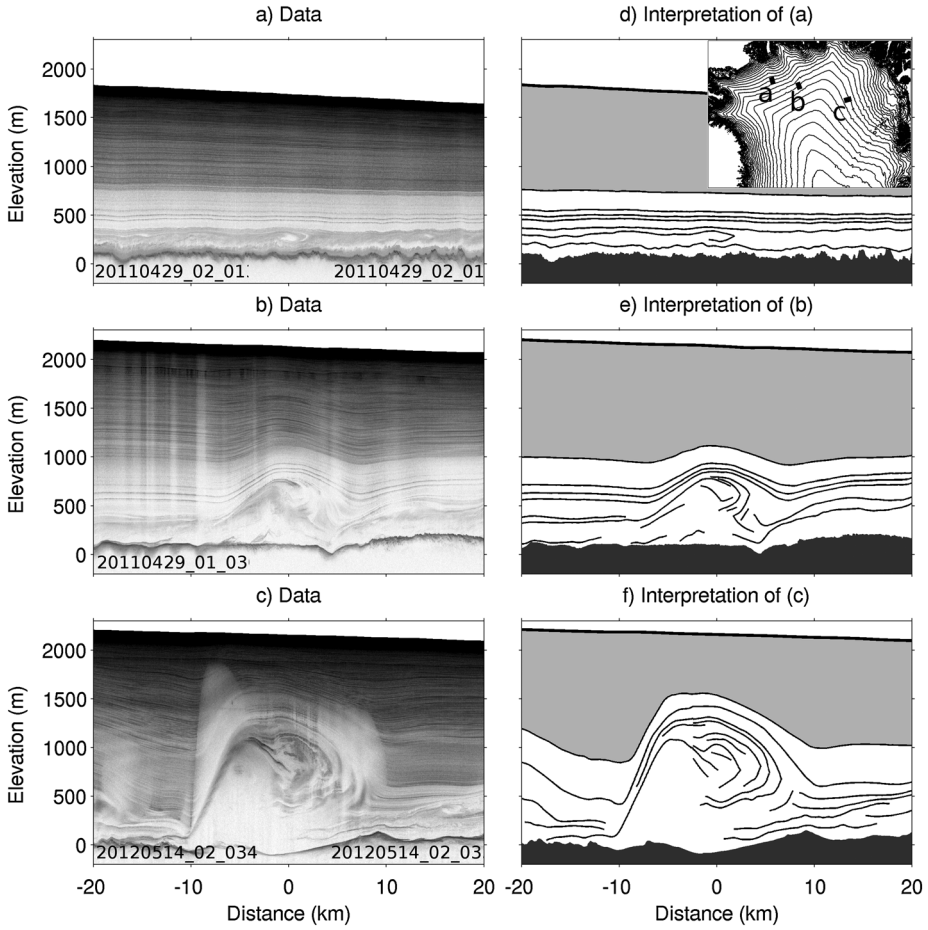

Figure 1. Overturned folds in ice-penetrating radar data from northern Greenland. (a) Small, (b) medium, and (c) large folds. (d–f) Stratigraphic interpretations. Radar data come from the CReSIS radar system on NASA's Operation IceBridge [*Li et al.*, 2013]. Identification numbers at the bottom of the echograms can be used to locate the radar data at data.cresis.ku.edu/data/rds. Englacial strata were picked with a hybrid manual/automatic picker. Light gray shading represents the densely layered Holocene stratigraphy. Bed and surface picks were taken as given from the CReSIS processing. Flow is from left to right in all panels. Figure 1c was also included in Figure 3c of *Bell et al.* [2014]. Inset map shows locations overlain on surface elevation contours. Vertical exaggeration is 10.

There are two ingredients necessary to produce overturned folds. First, there must be an initial stratigraphic disturbance, and second, that disturbance must be rolled over by englacial shear [*Waddington et al.*, 2001; *Jacobson and Waddington*, 2004, 2005]. An initial stratigraphic disturbance can be caused by a transient transition between basal slip and internal deformation. The change in ice velocity profile across this transition induces vertical flow that distorts ice sheet strata. This process, termed the "Weertman Effect" [*Weertman*, 1976; *Hindmarsh et al.*, 2006], has been used to study stationary transitions between sliding and internal deformation, such as those found on the shores of subglacial lakes [*Hindmarsh et al.*, 2006; *Parrenin and Hindmarsh*, 2007; *Leysinger Vieli et al.*, 2007]. When these transitions move downstream, a dynamic Weertman Effect is capable of producing large overturned basal folds [*Wolovick et al.*, 2014]. The second ingredient, englacial shear, is found above the sticky patches, where ice high in the column moves faster than ice near the bed. The difference in velocity with depth causes englacial disturbances to roll over [*Waddington et al.*, 2001]. Therefore, we focus on a single traveling sticky patch in order to better understand stratigraphic overturn.

In earlier work [*Wolovick et al.*, 2014], we described the behavior of traveling slippery patches moving through a background of sticky conditions. Here we analyze a traveling sticky patch moving through a background of slippery conditions. The moving reference frame analysis that we develop here could be applied to either a positive or a negative slip perturbation. We choose to analyze a sticky patch here because stratigraphic overturn requires the englacial shear that is found above a sticky patch.

2. Model

2.1. Kinematic Modeling Strategy

We use a kinematic model in a moving reference frame to systematically explore the relationship between traveling sticky patches and the stratigraphic folds they produce. We vary patch propagation velocity and the slip contrast between the patch and the far field. The tradeoff between basal slip and internal deformation is represented by using a linear superposition of a plug flow profile and a shear profile for the horizontal flow field. Mass conservation determines vertical velocity from the horizontal flow field.

We make several simplifying assumptions to render the problem tractable. We assume that the time dependence of basal sliding can be described by a temporally constant pattern propagating downstream over time. We neglect the effects of cross-flow divergence or convergence. Basal melting and freezing are set to zero. Ice thickness is assumed to be constant. In addition, the shear profile we use to represent internal deformation is a simple power law with depth, neglecting the effects of temperature, longitudinal stresses, and other variations in ice rheology.

Our model follows a single sticky patch in a moving reference frame as it travels downstream along an ice sheet flow line. The kinematic model in this approach has a small domain (approximately 40 km) and runs in a moving reference frame traveling at the same velocity as the sticky patch. By operating in a moving reference frame that follows the patch and the ice above it, we are able to gain a better understanding of the processes causing stratigraphy to fold and potentially overturn.

2.2. Mass Conservation

The mass conservation equation is expressed here in two dimensions as

$$\frac{\partial u}{\partial x} + \frac{\partial w}{\partial z} = 0, \tag{1}$$

where x is along-flow distance, z is elevation, u is horizontal velocity, w is vertical velocity, and cross-flow spreading has been assumed to be zero. Table 1 presents a summary of the symbols used in this paper.

2.3. Nondimensionalization and Coordinate Transformation

To transform into a moving reference frame, horizontal position is measured relative to the center of the traveling sticky patch, $x_c(t) = x_0 + u_p t$, where u_p is the patch propagation velocity and t is time. Distance and elevation are nondimensionalized by the ice thickness,

$$\hat{x} = \frac{x - x_c(t)}{H},$$

$$\hat{z} = \frac{z - B}{H}, \tag{2}$$

where H is ice thickness and B is bed elevation. Overhats indicate nondimensionalized variables. Time is nondimensionalized by the throughflow timescale for the ice thickness,

$$\hat{t} = \frac{\bar{u}_0 t}{H}, \tag{3}$$

where $\bar{u}_0$ is the column-average horizontal velocity at the starting location $x = x_0$. The column velocity increases downstream in balance with surface accumulation, so that in a stationary frame the column velocity is given by,

$$\bar{u}(x) = \bar{u}_0 + \frac{a}{H}(x - x_0), \tag{4}$$

where a is surface accumulation, expressed in ice-equivalent thickness. In the moving reference frame, column velocity is given by,

$$\bar{u}(\hat{x}, \hat{t}) = \bar{u}_0 + a\left(\hat{x} + \frac{x_c(\hat{t}) - x_0}{H}\right). \tag{5}$$

In a moving frame, the column velocity is a function of time, because the traveling patch is moving into regions of faster flow as it travels downstream.

Table 1. List of Symbols

Symbol	Formula	Units	Meaning
a	-	m/yr	surface accumulation rate
$\hat{a}$	$a/\bar{u}$	-	nondimensionalized accumulation rate
A	$aL/2\bar{u}_0 H$	-	accumulation index
B	-	m	bed elevation
h	$H\hat{h}$	m	thickness of overturning vortex
$\hat{h}$	$\hat{z}_t - \hat{z}_b$	-	nondimensionalized thickness of overturning vortex
H	-	m	ice thickness
k	-	-	overturning time constant
L	-	m	length of sticky patch
$\hat{L}$	L/H	-	nondimensionalized length of sticky patch
n	-	-	power law exponent for ice (=3)
P_e	$2\hat{h}^2\bar{u}H/k\hat{L}\kappa$	-	Péclet number
t	-	years	time
$\hat{t}$	$t\bar{u}_0/H$	-	nondimensionalized time
t_{over}	$kL/\bar{u}$	years	overturning time (one full rotation)
$\hat{t}_{over}$	$k\hat{L}$	-	nondimensionalized overturning time
u	-	m/yr	horizontal velocity
$\hat{u}$	$u/\bar{u} - \hat{u}_p$	-	nondimensionalized horizontal velocity
$\bar{u}$	-	m/yr	column-average horizontal velocity
$\bar{u}_0$	-	m/yr	column-average horizontal velocity at $x = x_0$
u_p	-	m/yr	sticky-patch propagation velocity
$\hat{u}_p$	$u_p/\bar{u}$	-	nondimensionalized propagation velocity
u_b	-	m/yr	basal sliding velocity
$\hat{u}_b$	$u_b/\bar{u}$	-	nondimensionalized sliding velocity
$\hat{u}_{ff}$	-	-	far-field velocity profile
w	-	m/yr	vertical velocity
$\hat{w}$	$w/\bar{u}$	-	nondimensionalized vertical velocity
x	-	m	horizontal coordinate
$\hat{x}$	$(x - x_c)/H$	-	nondimensionalized horizontal coordinate
x_c	-	m	center of traveling sticky patch
x_0	-	m	starting location of sticky patch
z	-	m	vertical coordinate
$\hat{z}$	$(z - B)/H$	-	nondimensionalized vertical coordinate
$\hat{z}_b$	-	-	bottom of overturning vortex (equation (11))
$\hat{z}_t$	-	-	top of overturning vortex (equation (12))
κ	-	$m^2\ s^{-1}$	thermal diffusivity of ice (= 1.4×10^{-6} $m^2\ s^{-1}$ [*Cuffey and Paterson*, 2010])
ϕ	-	-	lower throughflow (equations (10) and (14))

Horizontal velocity in the moving reference frame is measured relative to the propagation velocity of the traveling sticky patch, u_p. Both velocity components are nondimensionalized by the column velocity, resulting in

$$\hat{u}(\hat{x},\hat{z},\hat{t}) = \frac{u(x,z,t)}{\bar{u}(x)} - \hat{u}_p(\hat{t}),$$

$$\hat{w}(\hat{x},\hat{z},\hat{t}) = \frac{w(x,z,t)}{\bar{u}(x)}, \tag{6}$$

where $\hat{u}_p(\hat{t}) = u_p/\bar{u}(0,\hat{t})$ is the nondimensionalized patch propagation velocity. In this formulation we have assumed that the patch propagates at a constant absolute velocity, rather than a constant fraction of the

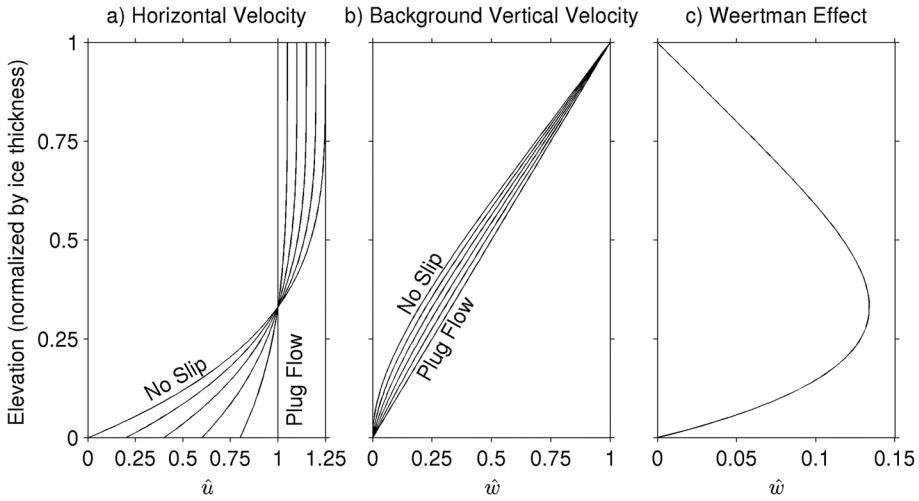

Figure 2. Velocity functions. (a) Horizontal velocity. (b) Background vertical velocity or the vertical flow that balances surface accumulation in steady state. (c) Weertman effect, or the vertical flow caused by the spatial gradient in basal slip. Figure 2a can be redimensionalized by multiplying by the column velocity, $\bar{u}$, Figure 2b can be redimensionalized by multiplying by the gradient in total ice flux, $-\partial(\bar{u}H)/\partial x$ (equal to surface accumulation in steady state), and Figure 2c can be redimensionalized by multiplying by the gradient in sliding flux, $-\partial(u_b H)/\partial x$. In Figures 2a and 2b a range of values of basal slip is shown. Note the scale change between Figures 2b and 2c.

ice column velocity. As a result, nondimensionalized propagation velocity decreases over time when surface accumulation is nonzero.

The nondimensionalized and transformed mass conservation equation then follows as

$$\frac{\partial \hat{u}}{\partial \hat{x}} + \frac{\partial \hat{w}}{\partial \hat{z}} + \frac{\hat{u}}{\bar{u}}\frac{\partial \bar{u}}{\partial \hat{x}} = 0, \tag{7}$$

where the additional term accounts for the gradient of the column velocity, and the gradient of ice thickness is assumed to be negligible.

2.4. Flow Field

Horizontal velocity is given by a linear superposition of sliding and internal deformation,

$$\hat{u}(\hat{x},\hat{z},\hat{t}) = \hat{u}_b(\hat{x}) + \left(1-\hat{u}_b(\hat{x})\right)\frac{n+2}{n+1}\left(1-(1-\hat{z})^{n+1}\right) - \hat{u}_p(\hat{t}), \tag{8}$$

where $\hat{u}_b(\hat{x}) = u_b(\hat{x},\hat{t})/\bar{u}(\hat{x},\hat{t})$ is the nondimensionalized sliding velocity and n is the rheological exponent for ice, taken to be 3 [*Cuffey and Paterson*, 2010]. We assume that the pattern of $\hat{u}_b(\hat{x})$ is constant over time when viewed in the moving reference frame. Examples of this flow field with different values of basal slip are shown in Figure 2a. When $\hat{u}_b = 1$, the ice sheet moves by a vertically uniform plug flow. As the sliding velocity $\hat{u}_b$ decreases, the shear profile in the lower part of the ice sheet becomes more pronounced and velocity in the upper part of the ice sheet increases to keep the average flow rate constant.

Once we have specified the horizontal component of velocity, we can use mass conservation to derive the vertical velocity component,

$$\hat{w}(\hat{x},\hat{z},\hat{t}) = \underbrace{-\hat{a}(\hat{x},\hat{t})\left[\frac{1-\hat{u}_b(\hat{x})}{n+1}\left(1-\hat{z}\right)^{n+2} + \left(\hat{u}_b(\hat{x}) + \left(1-\hat{u}_b(\hat{x})\right)\frac{n+2}{n+1}\right)\hat{z} - \frac{1-\hat{u}_b(\hat{x})}{n+1}\right]}_{\text{background vertical flow}}$$
$$\underbrace{-\frac{\mathrm{d}\hat{u}_b(\hat{x})}{\mathrm{d}\hat{x}}\frac{1}{n+1}\left(1-\hat{z}-(1-\hat{z})^{n+2}\right)}_{\text{Weertman effect}}, \tag{9}$$

where $\hat{a}(\hat{x},\hat{t}) = a/\bar{u}(\hat{x},\hat{t})$ is the nondimensionalized surface accumulation rate, and we have assumed that surface accumulation balances the gradient in column velocity. Nondimensionalized accumulation decreases over time because accumulation is constant while column velocity increases. The background vertical flow (Figure 2b) is the term that balances surface accumulation in a steady state. In a plug flow regime, the background vertical flow simply follows a linear gradient from the bed to the surface. When horizontal flow is by internal deformation, the background vertical flow profile is curved. The Weertman effect (Figure 2c) is the vertical velocity caused by the tradeoff between slip and deformation. The Weertman effect is zero at the bed and the surface, with a maximum in the ice column at an elevation about 30% above the bed. The vertical flow drops to zero at both the bed and the surface because the Weertman effect is a purely internal rearrangement of mass within the ice column.

2.5. Numerical Methods

We use a particle-tracking model to simulate ice sheet stratigraphy in a moving reference frame. The velocity field is constructed by using equations (5) and (8) to define $\bar{u}$ and $\hat{u}$, respectively. We combine $\hat{u}$ and $\bar{u}$ to compute u using equation (6), then compute w using equation (1). We set the initial column velocity $\bar{u}_0 = 1$. Strata are initially horizontal. When accumulation is set to zero, ice enters the domain only on the side boundaries, and new tracers are produced on the side boundaries at regular intervals. When accumulation is nonzero, ice also enters the domain at the top boundary, and the tracer production points on the side boundaries migrate downward over time in response to the background vertical velocity. The velocity field is interpolated linearly from an Eulerian grid onto the Lagrangian tracer locations. The model tracks the connectivity between tracers in coherent layers. We plot the stratigraphy using straight line segments connecting the tracers.

We use a model domain $20H$ long and we choose to investigate Gaussian sticky patches. A Gaussian function provides a smooth variation in the ice sheet flow field that approximates the averaging effects of longitudinal stress gradients that we do not include explicitly [*Kamb and Echelmeyer*, 1986]. We use a Gaussian with $\sigma = 2.5H$ as a representation of the longitudinal averaging scale. Changing the length of the sticky patch has no effect on the thickness of the overturning vortex when accumulation is low, because the thickness is controlled only by the difference between the sticky-patch velocity profile and the far-field velocity profile (section 3).

3. Stratigraphic Overturning

Stratigraphic overturning is caused by the balance of forward and backward flows in a moving reference frame. When viewed in a reference frame that moves with the traveling sticky patch, there is backward flow near the bed and forward flow higher in the column. Nonetheless, the total flux in the far-field ice column is the same as the total flux across the sticky patch. An example shown in Figure 3 has a propagation velocity greater than the far-field slip rate, so that the upstream and downstream velocity profiles both contain a small amount of reverse ice flux. Overturning occurs because the sticky–patch velocity profile has more reverse ice flux than these far-field profiles (Figure 3b). This additional reverse flow cannot escape into the far field and forms a vortex that traps and folds ice above the moving sticky patch.

To simplify the analysis, we ignore surface accumulation. Ignoring surface accumulation does three things: it makes the column velocity $\bar{u}(\hat{x},\hat{t})$ reduce to a constant, it eliminates the background vertical velocity, and it eliminates the time dependence of the velocity field when viewed in a moving reference frame. Later (section 4.3) we explore the effects of relaxing this assumption.

The forward and reverse fluxes as well as the boundaries of the trapped ice can be computed if the sticky-patch and far-field velocity profiles are known. The lower throughflow is the reverse flow in the far field, and it does not overturn (Figure 3). The lower throughflow, ϕ, is given by,

$$\phi = \int_{\hat{u}_{ff}<\hat{u}_p} (\hat{u}_{ff}(\hat{z}) - \hat{u}_p)\mathrm{d}\hat{z} \tag{10}$$

where $\hat{u}_{ff}(\hat{z})$ is the far-field velocity profile, and integration is over depths where the far-field velocity is less than the propagation velocity. In Figure 3b, ϕ is the thin red area near the bed, whereas in Figures 3a and 3c, ϕ is the red triangle to the left of the vertical line representing propagation velocity.

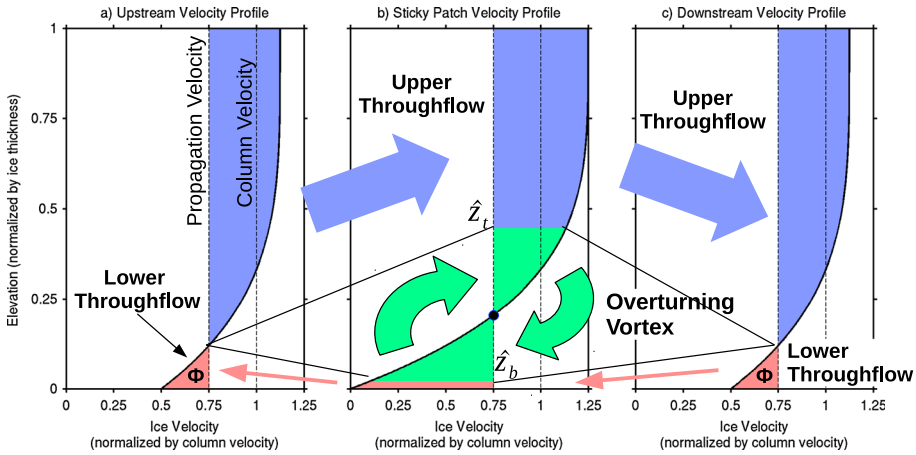

Figure 3. Schematic explanation of stratigraphic overturn above a traveling sticky patch. (a) Upstream velocity profile, (b) sticky-patch velocity profile, (c) downstream velocity profile. In this example the propagation velocity is 0.75 times the column velocity, the center of the sticky patch has no slip, and the far-field flow regime has half slip. The red and blue shadings represent throughflow, or the ice that moves past the sticky patch without becoming trapped in the overturning vortex. Green shading represents ice that is trapped within the overturning vortex. To conserve mass, the red and blue shadings must have the same area in all three plots, while the green shading must have equal positive and negative areas that sum to zero.

All of the areas representing the lower throughflow have equal magnitude in the three profiles. The bottom of the overturning vortex $\hat{z}_b$, is determined by the top of the lower throughflow in the sticky–patch velocity profile

$$\phi - \int_0^{\hat{z}_b} \left(\hat{u}(\hat{z}) - \hat{u}_p\right) \mathrm{d}\hat{z} = 0, \tag{11}$$

where the velocity profile $\hat{u}(\hat{z})$ used in the integration is taken from the center of the sticky patch. Equation (11) determines the boundary between the thin red lower throughflow in Figure 3b and the green trapped ice. The top of the vortex, $\hat{z}_t$, is determined by mass conservation as the elevation where forward and reverse flows balance one another:

$$\int_{\hat{z}_b}^{\hat{z}_t} \left(\hat{u}(\hat{z}) - \hat{u}_p\right) \mathrm{d}\hat{z} = 0. \tag{12}$$

If there is no reverse flow in the far field, then the vortex sits on the bed, and $\hat{z}_b = 0$. The remaining ice flow above the top of the vortex is the upper throughflow. The magnitude of the upper throughflow is equal to the forward ice flux in the far field.

We use equations (10)–(12) to solve for the top and bottom of the vortex as a function of the propagation velocity of the patch and the regional slip rate (Figure 4). The parameter space defined by those two variables is split into three separate regions depending on where the vortex is located in the ice column (Figure 4c). When the regional slip rate is faster than the propagation velocity, in the green region above the 1:1 line, there is no lower throughflow. The top of the vortex is a function of the propagation velocity only, indicated by vertical contours in Figure 4a, and the bottom of the vortex rests on the bed (Figure 4b).

In the narrow upper right red triangle, the overturning structure is in contact with the surface and there is no upper throughflow (Figure 4a). The diagonal line forming the left edge of this triangle is the line where propagation velocity is equal to far-field surface velocity. Folds in this region of parameter space have not been observed. Observations indicate that overturned folds are always in the lower portion of the ice sheet and never in contact with the surface.

When propagation velocity is greater than far-field slip rate and less than far-field surface velocity (lower blue triangle in Figure 4c) both an upper and a lower throughflow exist, meaning that the vortex is suspended in the middle of the ice column. However, the lower throughflow is thin and the bottom boundary is close to the bed (Figure 4b). In this region, contours of top and bottom elevation are both curved, indicating that

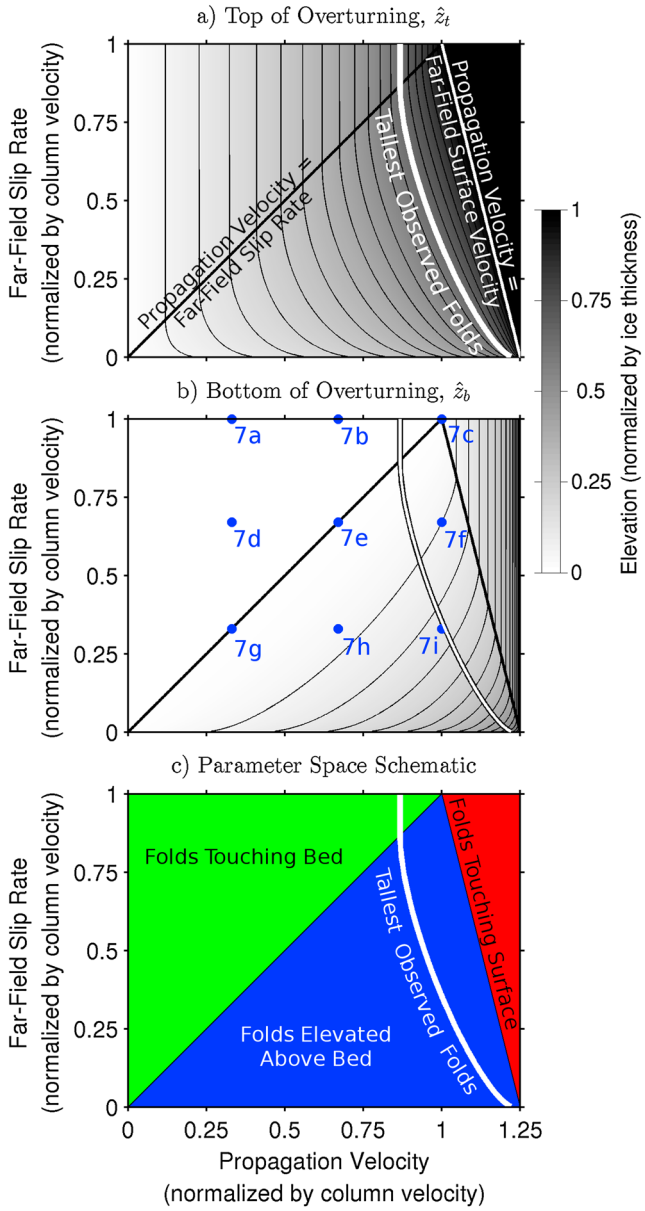

Figure 4. Dimensions of the overturning vortex as a function of the sticky-patch propagation velocity and of the far-field slip rate. (a) Top and (b) bottom of the overturning vortex. Thin black contour lines are shown with an interval of 0.05. (c) Schematic diagram of the important regions of parameter space. Parameter space is divided into a region where the overturning vortex is in contact with the bed (green), a region where the vortex is suspended in the ice column (blue), and a region where the vortex is in contact with the surface (red). Thick curved line indicates the approximate height of the tallest observed folds. Blue circles in Figure 4b show the locations of the model runs in Figure 7.

overturn geometry is a function of both propagation velocity and regional slip rate. The total thickness of the overturning vortex is largest when the sticky patch moves downstream at the far-field surface velocity.

In the preceding analysis, we assumed that the center of the sticky patch has no basal slip and ice moves completely by internal deformation. To get overturned folds when the sticky patch is weaker, higher propagation velocities and far-field slip rates are required. Weakening the sticky patch linearly shrinks the results in Figure 4 toward the point where propagation velocity and far-field slip rate both equal the ice column velocity (the point (1,1) in Figure 4). The shapes of the contours and the critical triangular regions in Figure 4c are unaffected by the slip rate in the sticky patch itself, they are simply confined to an increasingly small rectangle of parameter space around (1,1).

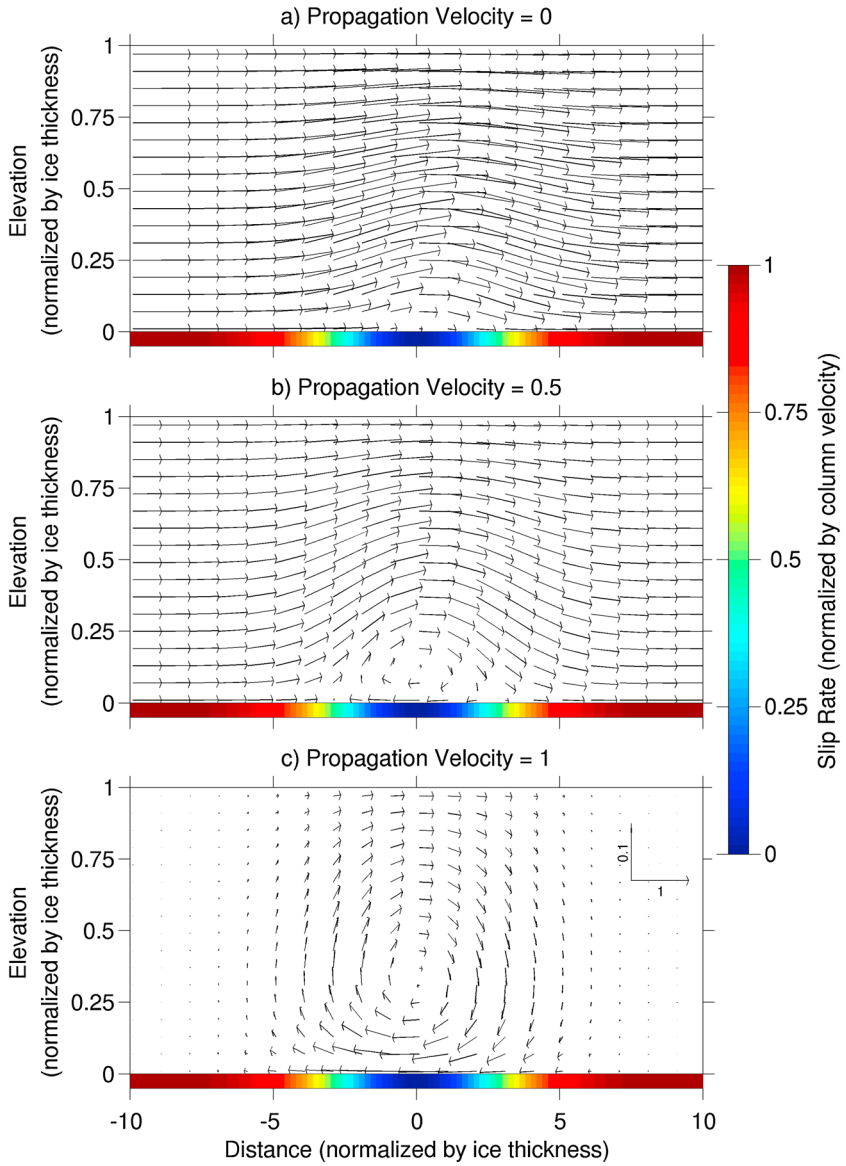

Figure 5. Velocity vectors in a moving reference frame. (a–c) Relative velocity field for a traveling sticky patch as the propagation velocity of the patch increases from 0 to 1. Color scale at the bottom of the plots shows the basal slip rate. The far-field flow regime is plug flow in these plots, corresponding to points along the upper border of the parameter space in Figure 4. Vertical exaggeration is 10.

4. Results

We investigate the relationship between traveling sticky patches and ice sheet stratigraphy. First, we show how the overturning vortex appears in velocity vectors in a moving reference frame. Next, we show stratigraphic snapshots as a function of time and for nine combinations of far-field slip rate and propagation velocity, based on Figure 4. We explore the effect of surface accumulation on overturned folds. Finally, we use this model to infer slip rates and propagation velocities based on measurements of fold geometry.

4.1. Velocity Vectors

The propagation velocity has a strong control on the form of the velocity field and the development of englacial vortices (Figure 5). When the propagation velocity is zero, the velocity field above the sticky patch simply reflects a shear profile within the ice, while velocity in the far-field is uniformly forward (Figure 5a). The stationary Weertman Effect produces only a small vertical deflection of the vectors in Figure 5a. When the sticky patch moves downstream, a vortex forms near the bed. Figure 5 shows how the size of the vortex

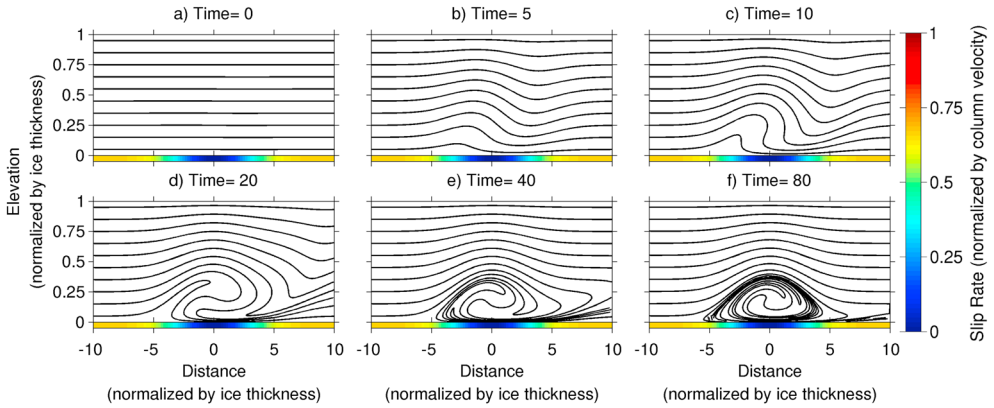

Figure 6. Time dependence of model stratigraphy. (a–f) Stratigraphic snapshots at increasing values of elapsed time. Figure 6a shows the initial condition and panels Figures 6b–6f show progressive doublings of elapsed time. This model run has a propagation velocity and a far-field slip rate of $\hat{u}_p = \hat{u}_{b,ff} = 2/3$, corresponding to Figure 7e. Color scale at the bottom of each panel indicates basal slip rate. Vertical exaggeration is 10.

responds to increasing propagation velocity when far-field slip rate is held constant. When the patch is propagating at half the ice column velocity (Figure 5b), ice near the bed moves slower than the propagation velocity, and therefore flows backward in the moving reference frame. The backward flowing ice is replenished by the downward limb of the vortex downstream of the sticky patch and feeds ice into the upward limb of the vortex upstream from the sticky patch. The entire vortex occupies roughly the lower quarter of the ice column, and flow vectors in the overlying ice are deflected vertically around the vortex. When propagation velocity equals the column velocity (Figure 5c), the overturning vortex expands to fill the entire ice column and velocity vectors in the far-field fall off to zero. The result is that the entire ice column is trapped above the traveling sticky patch. Though vortices spanning the full ice thickness are not observed, this result demonstrates that time-varying basal slip can have a very large impact on ice sheet stratigraphy.

4.2. Stratigraphy

As time progresses, initially horizontal strata above a traveling sticky patch become increasingly deformed (Figure 6). First, an anticline-syncline pair forms above the sticky patch, with the anticline upstream and the syncline downstream (Figure 6b). As time elapses, the fold limb connecting the anticline to the syncline steepens. The anticline becomes downstream verging and progresses from an inclined fold into a recumbent, or overturned, fold (Figures 6b–6d). Higher in the ice column, the initial syncline migrates downstream and escapes into the far-field, leaving an anticline centered over the patch (Figures 6c–6f). When the vortex near the bed has gone through approximately half a rotation from its initial state, strata in the lower part of the ice column form a single overturned fold (Figure 6d). Stratigraphic order changes twice within the overturned fold. Layers in the upper part of the fold young upward, layers in the middle of the fold young downward, and layers near the bed young upward again. When a large amount of time elapses, the lower part of the ice column overturns multiple times. Within this fold, alternating pairs of downward and upward younging stratigraphy develop in a concentric pattern around the center of the vortex. Strata in the upper part of the ice column reach a steady-state, symmetric anticline (Figure 6f). In contrast, strata in the vortex rotate indefinitely to produce loop-like structures (Figure 6f).

We next visualize stratigraphy for a variety of parameter combinations based on our analysis in section 3. We vary far-field slip rate and propagation velocity based on a grid in parameter space (Figure 4b). All of the model runs produce overturned folds in the lower part of the ice sheet and an anticline in the upper part (Figure 7). Additional model runs with a propagation velocity greater than $1.25\bar{u}$ produce a syncline at all depths with no overturned folds (not shown). Vortex size increases with both increasing far-field slip rate and increasing propagation velocity. Layers within the vortex approach the bed when far-field slip rate is greater than or equal to propagation velocity (Figures 7a–7e and 7g) because there is no lower throughflow. Conversely, a lower throughflow should be present when far-field slip rate is less than propagation velocity (Figures 7f, 7h, and 7i). In Figure 7i this can be seen as a subhorizontal layer above the bed but below the vortex. However, the use of a finite number of layers in the model makes it difficult to identify the thin lower throughflow in

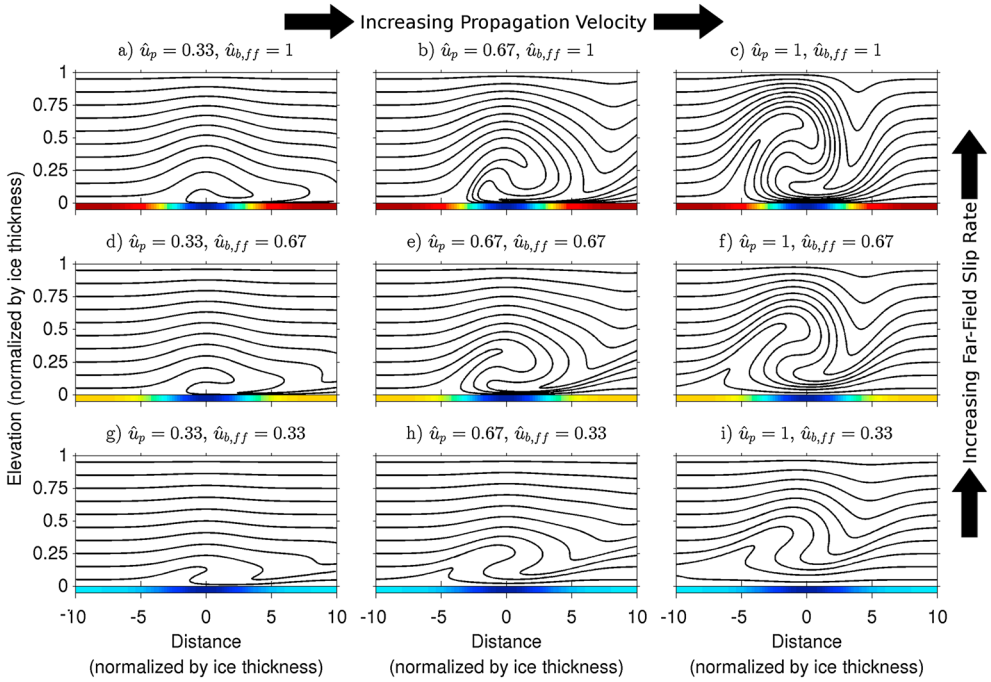

Figure 7. Model stratigraphy. (a–i) Stratigraphic snapshots after an elapsed time of 20 times $H/\bar{u}$. Labels above the plots give the sticky-patch propagation velocity, $\hat{u}_p$ and the far-field slip rate, $\hat{u}_{b,ff}$. Color scale at the bottom of each panel indicates basal slip rate with the same color scale as Figures 5 and 6. Labels at the top and right borders give the direction of increasing propagation velocity and far-field slip rate. Vertical exaggeration is 10.

Figures 7f and 7h. Figures 7c and 7f are outside the range of observed folds (Figure 4a), while the others are within the range of observations.

4.3. Surface Accumulation

We wish to estimate the thinning of the overturning vortex caused by surface accumulation. Surface accumulation has two main effects in our analysis: (1) accumulation produces a gradient in column velocity between the center of the sticky patch and the far field, and therefore produces a nonzero background vertical velocity; and 2) accumulation introduces a time dependence into the velocity field in the moving reference frame. We use the first effect to estimate a lower bound on the thickness of the overturning vortex in the presence of surface accumulation, then we use the numerical model to show how the second effect produces larger overturned folds than predicted by the first analysis.

We estimate a lower bound on the thickness of the vortex by using the initial velocity field in a modified version of the analysis in section 3. The initial velocity field has the lowest column velocity and therefore the highest relative accumulation ($\hat{a} = a/\bar{u}$). As the sticky patch propagates downstream, ice column velocity increases and the importance of accumulation relative to horizontal flow declines over time. To quantify the relative importance of accumulation, we introduce an accumulation index:

$$A = \frac{aL}{2\bar{u}_0 H}, \tag{13}$$

where L is the length of the sticky patch. The accumulation index is half the ratio between snow deposition over the patch and horizontal ice flux across the patch. Because of mass conservation, the index also represents the relative change in column velocity between the center of the sticky patch and the far field. We use the upstream velocity profile as the far-field velocity profile to compute the lower throughflow ϕ, following the analysis in section 3. Equation (10) then becomes

$$\phi = \int_{(1-A)\hat{u}_{ff} < \hat{u}_p} \left[(1-A)\,\hat{u}_{ff}(\hat{z}) - \hat{u}_p(0)\right] \mathrm{d}\hat{z}, \tag{14}$$

where the far-field velocity profile has been reduced by a factor of $(1 - A)$ relative to the zero accumulation case. Equation (11) is then used to define the bottom of the vortex $\hat{z}_b$ and equation (12) is used to define the

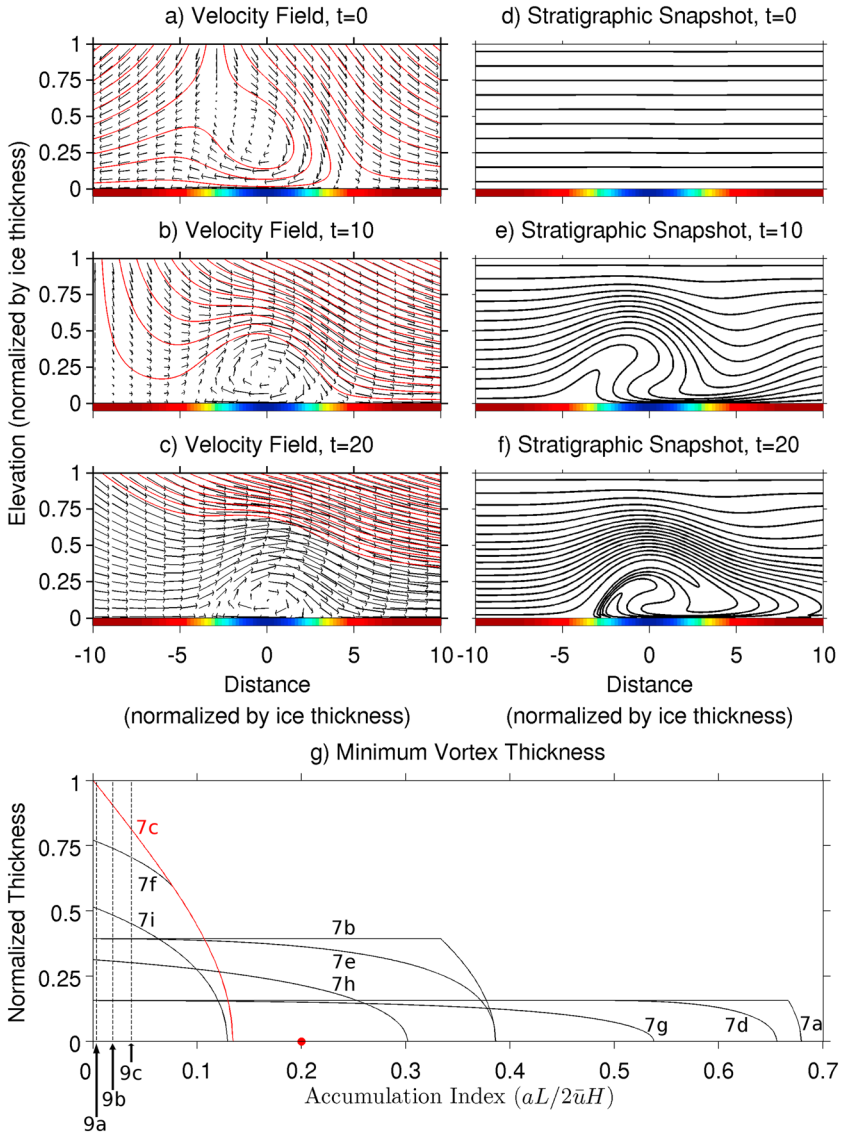

Figure 8. Influence of surface accumulation on stratigraphic overturn. (a–c) Snapshots of the velocity field above a traveling sticky patch in a moving reference frame with high accumulation ($A = 0.2$). Red lines show particle trajectories based on the instantaneous velocity field. (d–f) Snapshots of stratigraphy. (g) Minimum vortex thickness computed using equations (11), (12), and (14), ignoring the change in the velocity field over time. Calculations were performed for the same parameter grid used in Figure 7 and shown in Figure 4b. Figures 8a–8f in this figure use a parameter combination corresponding to Figure 7c, shown in red. Dashed lines show the value of A for the observational examples in Figure 9. Note that the calculations shown in Figure 8g predict that there should be no overturning vortex for the snapshots in this figure, but a small vortex forms anyway as the sticky patch propagates into a region of faster ice flow. Vertical exaggeration is 10.

top of the vortex $\hat{z}_t$. A slower far-field velocity profile produces more backward flow in the moving reference frame, and therefore ϕ is higher. Because ϕ is larger, $\hat{z}_b$ is higher, but $\hat{z}_t$ is lower, so that the overturning vortex is thinner than for the zero accumulation case. If A is large enough, the thickness of the overturning vortex drops to zero. The results of this minimum thickness analysis are shown in Figure 8g. The individual lines represent the same combinations of far-field slip rate and propagation velocity used in Figure 7.

The effect of increasing column velocity over time can be seen by comparing the instantaneous flow fields in Figures 8a–8c. In the initial condition (Figure 8a), the entire ice column at the upstream margin of the domain is flowing backward in the moving reference frame. Particle trajectories computed using the instantaneous velocity field originate at the surface and wrap partially around the vortex before escaping upstream. The minimum thickness analysis given above predicts no trapped overturning vortex here, consistent with the fact

that trajectories in the initial velocity field escape from the vortex into the far field. As time elapses (Figures 8b and 8c), the ice flow rate increases and the backward flow at the upstream margin disappears. A trapped overturning vortex reestablishes itself near the bed above the traveling sticky spot. Above the overturned folds (Figures 8d–8f), strata are compressed against the vortex as though it were a subglacial mountain. The overturned folds are smaller than they would have been without surface accumulation (compare Figure 8f with Figure 7c), but this reduction in size mostly reflects our assumption that the sticky patch propagates at a constant absolute velocity. Under that assumption, the relative propagation velocity $\hat{u}_p$ declines over time. If we had assumed that the sticky patch propagates at a constant fraction of the ice column velocity instead, then the reduction in vortex thickness would have been even less.

4.4. Interpretation of Observed Folds

We use the model presented above to interpret the stratigraphic folds in Figure 1 in terms of moving sticky patches. All three structures shown in Figure 1 are overturned folds in radar lines subparallel to flow. The angles between the flight lines in Figures 1a–1c and the ice flow direction are 3°, 19°, and 9°, respectively. The accumulation rates are 14, 17, and 10 cm/yr [*Noel et al.*, 2015]. Surface velocities are 33, 17, and 11 m/yr [*Joughin et al.*, 2010]. Basal topography is less than 10% of ice thickness, and basal melting or freezing rates are unknown. Additionally, ice in Greenland has rheological contrasts resulting from impurities, differing crystal sizes, and warmer temperatures near the bed [*NEEM Community Members*, 2013]. These environmental variables differ from the model assumptions of flow along track, no surface accumulation or basal melting, a flat bed, and a homogeneous power law rheology, but we proceed cautiously nonetheless.

The accumulation index, A, for the folds in Figures 1a–1c, is 0.004, 0.02, and 0.04, respectively. At these values of A, even the minimum thickness analysis predicts little change in overturn thickness for all but the largest folds (Figure 8g). Given that actual overturned folds are thicker than indicated by the minimum thickness analysis, and given that thermally controlled traveling sticky patches can keep pace with the ice column velocity rather than propagating at a constant absolute velocity [*Wolovick et al.*, 2014], we believe that ignoring surface accumulation in the succeeding analysis is a valid approximation.

These overturned folds appear to have bottom boundaries above the bed based on the presence of continuous reflectors underneath the largest limb of the fold. Bottom boundaries above the bed suggest that the propagation velocity is greater than the far-field slip rate (section 3). The larger two structures (Figures 1b and 1c) also push the upper layers into anticlines, although the smallest fold (Figure 1a) does not.

Regional slip rate and patch propagation velocity can be constrained relative to the ice column velocity by measuring the top and bottom boundaries of observed overturned folds. The "top" is defined as the highest point of the highest layer that can be traced to a layer overturn. We use this definition because it is compatible with the mass conservation equations used to define the boundaries of the overturning vortex (section 3). By using this definition we obtain higher estimates of fold amplitude than *Bell et al.* [2014]. The "top" defined here is a meteoric layer, as opposed to the lower disorganized scattering reflectors in the "basal units" [*Bell et al.*, 2014]. The uncertainty of the top measurement is the difference between the highest point of the uppermost overturned layer and the next traceable layer overlying it. The "bottom" is defined in a similar way, as the lowest point of the lowest layer that can be traced to a layer overturn. If a traceable layer cannot be found below the lowest overturned layer, the uncertainty of the bottom extends to the bed. Measurements of fold tops and bottoms are shown in Figures 9a–9c. The large fold in Figure 9c is big enough to have two bottom measurements, one each for the upstream and the downstream sides.

The measurements of fold top and bottom define permissible combinations of regional slip rate and patch propagation velocity (Figures 9d–9f). The measurements of fold top and bottom correspond to contours in Figure 4a and 4b, respectively. The uncertainty in the measurements corresponds to a set of parallel contours. When the fold is elevated above the bed, contours of constant top elevation and constant bottom elevation cross each other. The intersection of the contours defines a roughly trapezoidal shape in parameter space that is consistent with the observations for each fold.

We find that larger folds are produced by faster sticky patches and higher regional slip rates (Figures 9d–9f). The size of the three folds correlates with both increased far-field slip rate and increased propagation velocity. The dependence of fold amplitude on regional slip rate is weaker than the dependence on propagation velocity, resulting in more overlap between the examples. All three folds have a propagation velocity between approximately 0.5 and 1.0 times the column velocity. Only the downstream margin of the large fold could be

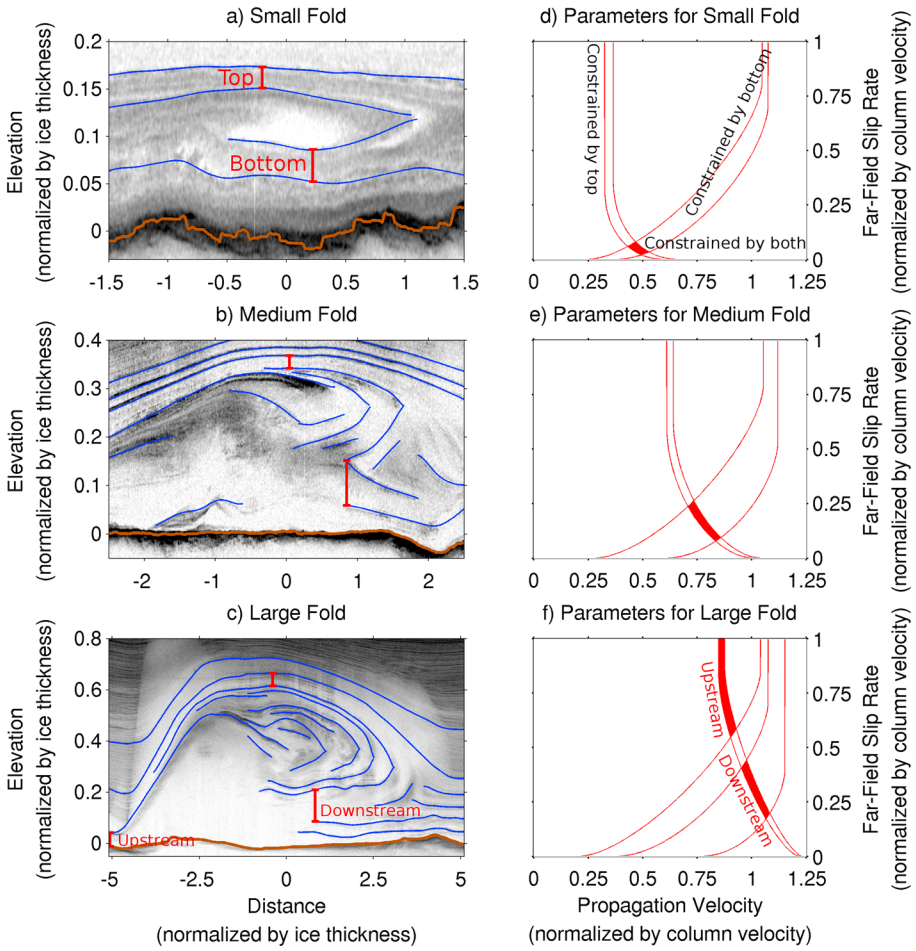

Figure 9. Measurements of the overturned folds in Figure 1 and corresponding constraints on parameter space. (a–c) Echograms with picks and measurements overlain. Images correspond to Figures 1a–1c. Note scale change to zoom in on overturned folds. (d–f) Parameter space corresponding to each fold. Red lines represent the constraints provided by the top or bottom of the fold separately, red shading represents the combined constraint.

consistent with a propagation velocity greater than the column velocity (Figure 9f). The two smaller folds and the downstream margin of the largest fold imply relatively low far-field slip rates of less than half the column velocity. However, the upstream margin of the largest fold is consistent with high sliding rates in the surrounding region.

Our results are consistent with the interpretation of *Bell et al.* [2014] that the largest fold (Figures 9c and 9f) is related to the freeze-on of basal water. Upstream of the fold, slip rates are high, indicating the presence of basal water. The uncertainty in the upstream measurement even allows for full plug flow. However, the low end of the uncertainty in upstream slip rate combined with the high end of the uncertainty of downstream slip rate implies only a small difference in slip rate. Underneath the center of the fold slip rate drops, consistent with loss of basal water, potentially due to freezing along the upstream margin of the fold. Downstream of the fold, slip rate recovers to an intermediate value of about a quarter to a half of the column velocity. In addition, in our model, the entire system of basal processes is traveling downstream at 80–100% of the velocity of the overlying ice column.

5. Discussion

Basal drag and slip are highly variable underneath ice sheets [e.g., *Sergienko et al.*, 2014]. We have shown that transitions between slip and stick produce large overturned folds for a wide range of far-field slip rates and patch propagation velocities. While we have chosen a simple power law rheology in our model, our results can be generalized to other ice rheologies. It is the transition between a shear profile and a plug flow profile

that produces folds. Therefore, we expect folds to be produced wherever basal slip gives way to internal deformation over short distances. If the transitions between slip and stick migrate downstream at a velocity comparable to the overlying ice sheet, folds become large and overturned.

Our results have direct implications for ice streams and their tributaries, where variations in driving stress and basal drag are especially pronounced [*Joughin et al.*, 2004, 2009; *Sergienko and Hindmarsh*, 2013; *Sergienko et al.*, 2014]. If sticky patches in the tributaries move, they will induce velocity vortices that yield folds. As ice flows into the main trunk of the stream, velocities increase dramatically [*Joughin et al.*, 2010; *Rignot et al.*, 2011]. If the sticky patches cannot match the increase in flow speed, then the stratigraphic structures become separated from the patches and are advected downstream. Longitudinal stretching will thin the folds over time, while internal deformation (if present) would augment the folds. Surface accumulation always compresses the folds downward. If there is little deformation then structures will advance as a coherent unit, crossing the grounding zone and potentially confounding interpretations of englacial stratigraphy there [*Christianson et al.*, 2013; *Bingham et al.*, 2015].

5.1. Three-Dimensional Effects

Cross-flow convergence or divergence modulates the influence of surface accumulation on the overturned folds produced by traveling sticky patches. Cross-flow divergence reduces the along-flow gradient of column velocity for a given accumulation rate, whereas cross-flow convergence increases the along-flow gradient of column velocity. Since the thinning effect of surface accumulation is partially counteracted by the tendency of a traveling patch to propagate into areas of faster ice flow over time (section 4.3), regions where flow converges will be more conducive to producing overturned folds. In three dimensions, there is also the possibility that sticky patches could propagate at an angle to flow, rather than straight downstream. The propagation of sticky patches will be affected by the movement of water along the bed, and this movement responds to changes in surface elevation. Thus, as surface elevation responds to variations in the divergence of ice flow, patch propagation rates and directions will respond as well. These effects may produce complicated folds that evolve as patch propagation changes in either magnitude or direction.

5.2. Folding Timescale

The time required for the overturning vortex to complete one full rotation is determined by comparing the volume of the trapped ice within the vortex with the one-way flux across the sticky patch (either the positive or the negative part of the green shading in Figure 3b). In general, the dimensionless overturn time is given by, $\hat{t}_{\text{over}} = k\hat{L}$, where $\hat{L} = L/H$ is the nondimensionalized length of the sticky patch and k is a constant that is a function of the propagation velocity, the far-field slip rate, the shape of the sticky-patch velocity profile, and the shape of the slip pattern $\hat{u}_b(\hat{x})$. For the Gaussian sticky patch and power law velocity profile we have used here, k ranges between about 3 and 20 for most of the parameter space we investigated (Figure 10). In dimensional terms, the overturn time is $t_{\text{over}} = kL/\bar{u}$ and the distance traveled by the sticky patch during that time is $\Delta x = u_p t_{\text{over}} = kL\hat{u}_p$. For the folds observed in the interior of northern Greenland, lengths of the active portion tend to be in the range 10–30 km and ice velocity ranges from 1 to 100 m/yr [*Bell et al.*, 2014]. Thus, the overturn timescale ranges between 150 and 300,000 years and the propagation distance is 0–300 km, where we have used a value of $k/2$ to represent roughly half a rotation. These propagation distances give ample space for an overturned fold to develop in the interior of the ice sheet before a sticky patch reaches the margin. The high end of the range of potential overturn times is larger than the thermal diffusion timescale for the ice sheet ($\sim 10^5$ years), larger than the accumulation timescale ($H/a \sim 10^4$ years), and larger than the timescale of glacial-interglacial climate variability ($\sim 10^5$ years). In contrast, the low end of the range is essentially instantaneous compared to those timescales.

5.3. Thermal Overturn

Thermal structure near the bed exerts a critical control on ice flow, deformation, basal melting, and water transport. If stratigraphic overturn happens more rapidly than thermal diffusion, then the strata will carry their temperature structure with them as they rotate and the ice sheet will develop a temperature inversion. As layers fold in the overturning vortex, initially horizontal isotherms will be advected and become overturned as well. If stratigraphic overturn happens slowly compared to thermal diffusion, then isotherms will remain approximately horizontal.

To quantify the potential for thermal overturn, we define a Péclet number by comparing the timescale for thermal diffusion for heat out of the vortex with the timescale for stratigraphic overturn. The timescale for overturn, given above, is $kL/2\bar{u}$, where we have inserted a factor of 1/2 to represent a single overturn caused

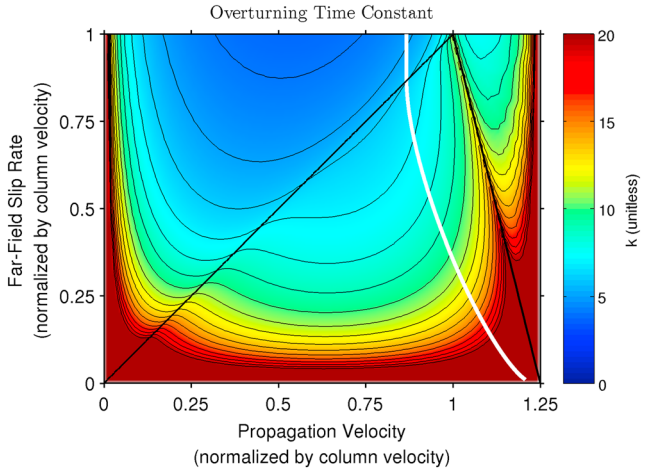

Figure 10. Dimensionless time constant, k, for the overturning vortex that forms above a Gaussian sticky patch. Color scale saturates at 20, although k approaches infinity as the size of the overturning vortex approaches zero. k is calculated by computing the volume of trapped ice and dividing by the one-way flux within the trapped region of the sticky-patch velocity profile (either the positive or the negative part of the green shading in Figure 3b). Time represents the time required for one complete rotation of the overturning vortex. Note that many observed folds have only a single overturn, corresponding to half a rotation. In order to produce this figure, the length of the Gaussian sticky patch was defined to be 4σ (i.e., its extent was defined as $\pm 2\sigma$). Thin lines represent contours of k. As in Figure 4, the diagonal lines represent the 1:1 line and the line where propagation velocity equals far-field surface velocity, while the thick curved line represents the largest observed folds.

by half a rotation. The timescale for diffusion is h^2/κ, where κ is the thermal diffusivity of ice and h is the thickness of the overturning vortex. We represent h in terms of the ice thickness, $h = \hat{h}H$, where $\hat{h} = \hat{z}_t - \hat{z}_b$ is the nondimensionalized thickness of the vortex. We then use the ratio of the diffusion timescale to the overturn timescale to define the Péclet number,

$$P_e = \left(\frac{2\hat{h}^2}{k\hat{L}}\right)\frac{\bar{u}H}{\kappa}. \tag{15}$$

To compute a broad range of possible Péclet numbers, we define maximum and minimum values of the input parameters based on the range of observed folds [*Bell et al.*, 2014]: $\hat{h}$ ranges from 0.05 to 0.67, k ranges from 3 to 20, $\hat{L}$ ranges from 1 to 10, H ranges from 2000 m to 3000 m, $\bar{u}$ ranges from 1 m/yr to 100 m/yr, and κ is 1.4×10^{-6} m^2 s^{-1} [*Cuffey and Paterson*, 2010]. Based on these values, P_e ranges from $1{\times}10^{-3}$ to $2{\times}10^{3}$, although this range may overstate the variability because high values of $\hat{h}$ are generally associated with high values of $\hat{L}$. To compute a tighter range of possible Péclet numbers, we compute P_e for the three specific folds that we analyzed in section 4.4. Those folds all have a Péclet number within an order of magnitude of unity: 0.3–1.3 for the small fold in Figure 9a, 1.0–4.4 for the medium–sized fold in Figure 9b, and either 1.3–4.6 or 5.4–12.0 for the large fold in Figure 9c, depending on whether we use the downstream or the upstream measurement for the bottom boundary of the fold.

Values of the Péclet number much larger than unity indicate that advection dominates over diffusion and thermal overturn is likely, while low values indicate that stratigraphic overturn should have little effect on the ice sheet thermal structure. Values close to unity indicate that both advection and diffusion are important within the overturned fold. If thermal overturn occurs, boreholes drilled through actively overturning stratigraphic folds should measure a temperature inversion, with cold ice underneath warm ice in the lower third of the ice column. Repeated stratigraphic overturns may produce a nearly isothermal layer in the bottom of the ice sheet, as the thermal structure of the fold is homogenized by mechanical mixing.

Thermal overturn reinforces a traveling sticky patch, creating a positive feedback. Cold ice near the bed increases conductive cooling that promotes basal freeze-on, results in loss of basal water, and yields a reduction in sliding. Conductive cooling and basal freeze-on require a thin conductive boundary layer to be present near the bed even if the bulk of the vortex is dominated by advection. Subglacial freeze-on resulting from thermal overturn could cause a sticky patch to continuously dewater the bed as it travels downstream. Thermal overturn compliments the mechanism for downstream propagation described by *Wolovick et al.* [2014] and provides an explanation for how the patches can strengthen over time.

Ice sheet temperature and the distribution of basal water are difficult to constrain. The most reliable results come from borehole measurements, but the distribution of these is extremely sparse. Indirect estimates of temperature in the upper part of the ice column may be made from measurements of radar attenuation rate [*MacGregor et al.*, 2015b]. Basal water has been constrained by radar reflectivity estimates using column-average attenuation rates that often do not account for variable thermal structure [e.g., *Oswald and Gogineni*, 2008; *Wolovick et al.*, 2013; *Jacobel et al.*, 2010; *Carter et al.*, 2007], even though attenuation is highly sensitive to warm ice near the bed [*MacGregor et al.*, 2012; *Matsuoka*, 2011]. Our model indicates that ice sheet thermal structure in the vicinity of overturned stratigraphic folds may be extremely complex, including warm attenuating ice higher in the ice column. Folds can cause laterally and vertically variable attenuation in the ice column, making interpretation of both englacial and bed echoes more challenging.

5.4. Ice Cores

Near the center of ice sheets, ice cores show disturbances near the bed. Strong variations between isotope records [*Grootes et al.*, 1993] and corroborated by flow microstructures suggest deformational processes [e.g., *Montagnat et al.*, 2014; *Dahl-Jensen et al.*, 1997; *Faria et al.*, 2010]. Observations from the NEEM core in Greenland [*NEEM Community Members*, 2013] and the differences in the cores between the GRIP and GISP2 records [*Grootes et al.*, 1993] suggest folding. Notably, there are even rib-like variations in driving stress along the ice divide in Greenland, suggesting variations in basal resistance there [*Sergienko et al.*, 2014]. These ribs could give rise to large overturned folds, but we note that our mechanism cannot give the exact results seen at NEEM because a stratigraphic discontinuity is observed there and our model is a continuum flow model. However, folding at various scales is a ubiquitous feature of the deep ice core record [*Grootes et al.*, 1993; *Montagnat et al.*, 2014; *Faria et al.*, 2010; *NEEM Community Members*, 2013], and some of those folds may be due to traveling sticky patches.

5.5. Relationship to Other Mechanisms

Three mechanisms have been proposed to explain the observed stratigraphic structures in Greenland and Antarctica: basal freeze-on [*Bell et al.*, 2011], traveling slippery or sticky patches [*Wolovick et al.*, 2014], and rheological contrasts within the ice column [*NEEM Community Members*, 2013]. It is likely that different mechanisms are dominant to various degrees in different structures, and some structures may be the result of multiple mechanisms acting simultaneously. Here we have examined traveling sticky patches in detail. The question of how multiple mechanisms might interact with each other remains unexplored. For example, basal freeze-on may act to dewater the bed, increasing basal drag and reducing slip rate. In return, thermal overturn may bring cold ice close to the bed, encouraging basal freeze-on and ensuring that a traveling sticky patch remains sticky as it travels. Only a small thickness of freeze-on ($\sim$10 m) is required to drastically reduce slip rate [*Christoffersen et al.*, 2010], so refrozen ice need not occupy a large fraction of the resulting englacial fold. Rheological heterogeneity in the ice column will modify the shape of the velocity profile above a sticky patch, changing the thickness of the overturning vortex relative to what we have calculated here. In return, rheological contrasts will be displaced by the rotating vortex, modifying the sticky-patch deformation profile and the vortex velocity field over time. The interaction between all three mechanisms could potentially lead to new dynamic feedbacks not captured by simple models.

5.6. Observational Constraints

The range of allowable parameter space for traveling sticky patches can be constrained by comparing model stratigraphic structures with observed stratigraphic structures. Overturned folds are always found nearer to the bed than the surface [*Bell et al.*, 2011, 2014; *MacGregor et al.*, 2015a], discounting the red region in Figure 4. In addition, the tops of the observed folds are usually less than half of the ice thickness [*Bell et al.*, 2014]. The fold shown in Figure 1c, at approximately two thirds of the ice thickness, represents the extreme high end of the range of observed overturned folds. This upper limit is shown by the thick curved line in Figure 4. All observed folds fall to the left of this curve, indicating that the sticky patches that produce overturned folds usually propagate at less than the ice column velocity. There is some uncertainty from the measurements, suggesting that the fastest sticky patches could propagate slightly faster than the column velocity (Figure 9f). In addition, sticky patches propagating faster than the local surface velocity ($1.25\bar{u}$ in Figure 4) are also consistent with the observations, although we have not focused on fast sticky patches because they do not produce overturned folds. Sticky patches propagating faster than the local surface velocity produce a syncline at all depths instead of overturned folds, and synclines are commonly observed in the Greenland ice sheet [e.g., *MacGregor et al.*, 2015a]. The range of allowable parameter space therefore includes both the area to the

left of the thick curved line labeled "Tallest Observed Folds" in Figure 4, and everything off the chart to the right. The wedge-shaped region between the curved line and the right margin of the plot is not supported by observations.

Many of the observed overturned folds have both distinct tops and distinct bottoms, implying that the patch propagation velocity is greater than far-field slip rate. Observations of the bottom boundaries of overturned folds are crucial for interpreting regional slip rates. Bottom observations are both difficult to acquire because of increasing radar attenuation and geometric spreading deeper in the ice sheet and difficult to interpret because of the complexity of reflectors near the bed. The interpretation of reflectors underneath the overturned folds suggests that a lower throughflow is present. The presence of a lower throughflow implies that internal deformation is an important contributor to bulk ice flow in the region surrounding the folds.

6. Conclusions

Traveling sticky patches produce overturning vortices in the lower part of the ice sheet when viewed in a moving reference frame. The vortices produce overturned stratigraphic folds that rotate over time. Ice within overturning vortices is trapped above the moving sticky patch, allowing the thickness of the vortex to be calculated by mass conservation. The overturning vortices are largest when the patch moves downstream at the regional surface velocity (Figure 4). Traveling sticky patches can produce overturned folds at any elevation within the ice column, from the bed to the surface, although folds near the bed are more likely. As a result, measurements of the upper and lower boundaries of observed overturned folds can be used to constrain the parameter range of real traveling sticky patches. Three example folds were measured and all three could have been produced by sticky patches moving at a velocity between 0.5 and 1.0 times the ice column velocity. In addition, the observation that many overturned folds have a bottom boundary raised above the bed implies that internal deformation is an important contributor to bulk ice flow in northern Greenland in addition to basal slip. Ice sheet stratigraphy responds strongly to both traveling slippery patches and traveling sticky patches, leaving a record of the temporal variability in basal slip encoded in the layers of the overlying ice sheet.

Acknowledgments
We thank the members of CReSIS and Operation IceBridge for collecting and processing the radar data shown in this paper. We thank Robin E. Bell and W. Roger Buck for thoughtful comments on earlier versions of the manuscript. M.J.W. was supported by a NASA Earth and Space Science Fellowship (14-EARTH14R-67). T.T.C. was supported by the Lamont-Doherty Earth Observatory and NSF grant 1043481.

References

Bamber, J. L., et al. (2013), A new bed elevation dataset for Greenland, *Cryosphere*, *7*(2), 499–510, doi:10.5194/tc-7-499-2013.
Bell, R., et al. (2011), Widespread persistent thickening of the East Antarctic Ice Sheet by freezing from the base, *Science*, *331*(6024), 1592–1595, doi:10.1126/science.1200109.
Bell, R. E., K. Tinto, I. Das, M. Wolovick, W. Chu, T. T. Creyts, N. Frearson, A. Abdi, and J. D. Paden (2014), Deformation, warming and softening of Greenland's ice by refreezing meltwater, *Nat. Geosci.*, *7*(7), 497–502, doi:10.1038/ngeo2179.
Bingham, R. G., D. M. Rippin, N. B. Karlsson, H. F. J. Corr, F. Ferraccioli, T. A. Jordan, A. M. Le Brocq, K. C. Rose, N. Ross, and M. J. Siegert (2015), Ice-flow structure and ice dynamic changes in the Weddell Sea sector of West Antarctica from radar-imaged internal layering, *J. Geophys. Res. Earth Surf.*, *120*, 655–670, doi:10.1002/2014JF003291.
Carter, S., D. Blankenship, M. Peters, D. Young, J. Holt, and D. Morse (2007), Radar-based subglacial lake classification in Antarctica, *Geochem. Geophys. Geosyst.*, *8*, Q03016, doi:10.1029/2006GC001408.
Christianson, K., B. R. Parizek, R. B. Alley, H. J. Horgan, R. W. Jacobel, S. Anandakrishnan, B. A. Keisling, B. D. Craig, and A. Muto (2013), Ice sheet grounding zone stabilization due to till compaction, *Geophys. Res. Lett.*, *40*, 5406–5411, doi:10.1002/2013GL057447.
Christoffersen, P., S. Tulaczyk, and A. Behar (2010), Basal ice sequences in Antarctic ice stream: Exposure of past hydrologic conditions and a principal mode of sediment transfer, *J. Geophys. Res.*, *115*, F03034, doi:10.1029/2009JF001430.
Cuffey, K., and W. Paterson (2010), *The Physics of Glaciers*, 4th ed., Butterworth-Heineman/Elsevier, Burlington, Mass.
Dahl-Jensen, D., T. Thorsteinsson, R. Alley, and H. Shoji (1997), Flow properties of the ice from the Greenland Ice Core Project ice core: The reason for folds?, *J. Geophys. Res.*, *102*(C12), 26,831–26,840, doi:10.1029/97JC01266.
Dansgaard, W., and S. Johnson (1969), A flow model and a timescale for the ice core from Camp Century, Greenland, *J. Glaciol.*, *8*(53), 215–223.
Faria, S. H., J. Freitag, and S. Kipfstuhl (2010), Polar ice structure and the integrity of ice-core paleoclimate records, *Quat. Sci. Rev.*, *29*(1–2), 338–351, doi:10.1016/j.quascirev.2009.10.016.
Fretwell, P., et al. (2013), Bedmap2: Improved ice bed, surface and thickness datasets for Antarctica, *Cryosphere*, *7*(1), 375–393, doi:10.5194/tc-7-375-2013.
Grootes, P. M., M. Stuiver, J. W. C. White, S. Johnsen, and J. Jouzel (1993), Comparison of oxygen isotope records from the GISP2 and GRIP Greenland ice cores, *Nature*, *366*(6455), 552–554, doi:10.1038/366552a0.
Hindmarsh, R. C., G. J. Leysinger Vieli, M. J. Raymond, and G. H. Gudmundsson (2006), Draping or overriding: The effect of horizontal stress gradients on internal layer architecture in ice sheets, *J. Geophys. Res.*, *111*, F02018, doi:10.1029/2005JF000309.
Jacobel, R. W., K. E. Lapo, J. R. Stamp, B. W. Youngblood, B. C. Welch, and J. L. Bamber (2010), A comparison of basal reflectivity and ice velocity in East Antarctica, *Cryosphere*, *4*(4), 447–452, doi:10.5194/tc-4-447-2010.
Jacobson, H., and E. Waddington (2005), Recumbent folding of divide arches in response to unsteady ice-divide migration, *J. Glaciol.*, *51*(173), 201–209, doi:10.3189/172756505781829412.
Jacobson, H. P., and E. D. Waddington (2004), Recumbent folding in ice sheets: A core-referential study, *J. Glaciol.*, *50*(168), 3–16, doi:10.3189/172756504781830204.

Joughin, I., D. MacAyeal, and S. Tulaczyk (2004), Basal shear stress of the Ross ice streams from control method inversions, *J. Geophys. Res.*, *109*, B09405, doi:10.1029/2003JB002960.

Joughin, I., S. Tulaczyk, J. L. Bamber, D. Blankenship, J. W. Holt, T. Scambos, and D. G. Vaughan (2009), Basal conditions for Pine Island and Thwaites Glaciers, West Antarctica, determined using satellite and airborne data, *J. Glaciol.*, *55*(190), 245–257, doi:10.3189/002214309788608705.

Joughin, I., B. E. Smith, I. M. Howat, T. Scambos, and T. Moon (2010), Greenland flow variability from ice-sheet-wide velocity mapping, *J. Glaciol.*, *56*(197), 415–430, doi:10.3189/002214310792447734.

Kamb, B., and K. Echelmeyer (1986), Stress-gradient coupling in glacier flow. 1. Longitudinal averaging of the influence of ice thickness and surface slope, *J. Glaciol.*, *32*(111), 267–284.

Leysinger Vieli, G., R. Hindmarsh, and M. Siegert (2007), Three-dimensional flow influences on radar layer stratigraphy, *Ann. Glaciol.*, *46*(1), 22–28, doi:10.3189/172756407782871729.

Li, J., J. Paden, C. Leuschen, F. Rodriguez-Morales, R. D. Hale, E. J. Arnold, R. Crowe, D. Gomez-Garcia, and P. Gogineni (2013), High-altitude radar measurements of ice thickness over the Antarctic and Greenland Ice Sheets as a part of Operation IceBridge, *IEEE Trans. Geosci. Remote Sens.*, *51*(2), 742–754, doi:10.1109/TGRS.2012.2203822.

MacGregor, J. A., K. Matsuoka, E. D. Waddington, D. P. Winebrenner, and F. Pattyn (2012), Spatial variation of englacial radar attenuation: Modeling approach and application to the Vostok flowline, *J. Geophys. Res.*, *117*, F03022, doi:10.1029/2011JF002327.

MacGregor, J. A., M. A. Fahnestock, G. A. Catania, J. D. Paden, S. Prasad Gogineni, S. K. Young, S. C. Rybarski, A. N. Mabrey, B. M. Wagman, and M. Morlighem (2015a), Radiostratigraphy and age structure of the Greenland Ice Sheet, *J. Geophys. Res. Earth Surf.*, *120*, 212–241, doi:10.1002/2014JF003215.

MacGregor, J. A., et al. (2015b), Radar attenuation and temperature within the Greenland Ice Sheet, *J. Geophys. Res. Earth Surf.*, *120*, 983–1008, doi:10.1002/2014JF003418.

Matsuoka, K. (2011), Pitfalls in radar diagnosis of ice-sheet bed conditions: Lessons from englacial attenuation models, *Geophys. Res. Lett.*, *38*, L05505, doi:10.1029/2010GL046205.

Montagnat, M., N. Azuma, D. Dahl-Jensen, J. Eichler, S. Fujita, F. Gillet-Chaulet, S. Kipfstuhl, D. Samyn, A. Svensson, and I. Weikusat (2014), Fabric along the NEEM ice core, Greenland, and its comparison with GRIP and NGRIP ice cores, *Cryosphere*, *8*(4), 1129–1138, doi:10.5194/tc-8-1129-2014.

NEEM Community Members (2013), Eemian interglacial reconstructed from a Greenland folded ice core, *Nature*, *493*(7433), 489–494, doi:10.1038/nature11789.

Noel, B., W. J. van de Berg, E. van Meijgaard, P. Kuipers Munneke, R. S. W. van de Wal, and M. R. van den Broeke (2015), Evaluation of the updated regional climate model RACMO2.3: Summer snowfall impact on the Greenland Ice Sheet, *Cryosphere*, *9*(5), 1831–1844, doi:10.5194/tc-9-1831-2015.

Oswald, G., and S. Gogineni (2008), Recovery of subglacial water extent from Greenland radar survey data, *J. Glaciol.*, *54*(184), 94–106, doi:10.3189/002214308784409107.

Parrenin, F., and R. Hindmarsh (2007), Influence of a non-uniform velocity field on isochrone geometry along a steady flowline of an ice sheet, *J. Glaciol.*, *53*(183), 612–622, doi:10.3189/002214307784409298.

Rignot, E., J. Mouginot, and B. Scheuchl (2011), Ice flow of the Antarctic Ice Sheet, *Science*, *333*(6048), 1427–1430, doi:10.1126/science.1208336.

Sergienko, O. V., and R. C. A. Hindmarsh (2013), Regular patterns in frictional resistance of ice-stream beds seen by surface data inversion, *Science*, *342*(6162), 1086–1089, doi:10.1126/science.1243903.

Sergienko, O. V., T. T. Creyts, and R. C. A. Hindmarsh (2014), Similarity of organized patterns in driving and basal stresses of Antarctic and Greenland ice sheets over extensive areas of basal sliding, *Geophys. Res. Lett.*, *41*, 3925–3932, doi:10.1002/2014GL059976.

Waddington, E., J. Bolzan, and R. Alley (2001), Potential for stratigraphic folding near ice-sheet centers, *J. Glaciol.*, *47*(159), 639–648, doi:10.3189/172756501781831756.

Weertman, J. (1976), Sliding-no sliding zone effect and age determination of ice cores, *Quat. Res.*, *6*(2), 203–207, doi:10.1016/0033-5894(76)90050-8.

Wolovick, M. J., R. E. Bell, T. T. Creyts, and N. Frearson (2013), Identification and control of subglacial water networks under Dome A, Antarctica, *J. Geophys. Res. Earth Surf.*, *118*, 140–154, doi:10.1029/2012JF002555.

Wolovick, M. J., T. T. Creyts, W. R. Buck, and R. E. Bell (2014), Traveling slippery patches produce thickness-scale folds in ice sheets, *Geophys. Res. Lett.*, *41*(24), 8895–8901, doi:10.1002/2014GL062248.